EBioMedicine 19 (2017) 49–59

Contents lists available at ScienceDirect

EBioMedicine

journal homepage: www.ebiomedicine.com

Research Paper

Fluvastatin Prevents Lung Adenocarcinoma Bone Metastasis by Triggering Autophagy

Zuozhang Yang [a,*,1], Zhenyi Su [b,c,**,1], Judy Park DeWitt [c,1], Lin Xie [d], Yongbin Chen [e], Xiaojuan Li [a], Lei Han [a], Dongqi Li [a], Junfeng Xia [a], Ya Zhang [a], Yihao Yang [a], Congguo Jin [f], Jing Zhang [a], Su Li [a], Kun Li [g], Zhiping Zhang [g], Xin Qu [a], Zewei He [a], Yanjin Chen [a], Yan Shen [d], Mingyan Ren [d], Zhongqin Yuan [d]

[a] Bone and Soft Tissue Tumors Research Center of Yunnan Province, Department of Orthopaedics, The Third Affiliated Hospital of Kunming Medical University (Tumor Hospital of Yunnan Province), Kunming, Yunnan 650118, China
[b] Department of Biochemistry and Molecular Biology, Medical School, Southeast University, Nanjing, Jiangsu 210009, China
[c] Department of Cell Biology, Harvard Medical School, Boston, MA 02115, USA
[d] Department of Medical Oncology, The Third Affiliated Hospital of Kunming Medical University (Tumor Hospital of Yunnan Province), Kunming, Yunnan 650118, China
[e] Key Laboratory of Animal Models and Human Disease Mechanisms, Kunming Institute of Zoology, Chinese Academy of Sciences, Kunming, Yunnan 650223, China
[f] Cancer Institute, The Third Affiliated Hospital of Kunming Medical University (Tumor Hospital of Yunnan Province), Kunming, Yunnan 650118, China
[g] Department of Radiology, The Third Affiliated Hospital of Kunming Medical University (Tumor Hospital of Yunnan Province), Kunming, Yunnan 650118, China

ARTICLE INFO

Article history:
Received 11 December 2016
Received in revised form 6 April 2017
Accepted 10 April 2017
Available online 11 April 2017

Keywords:
Fluvastatin
Autophagy
Lung adenocarcinoma bone metastasis
Statins
p53

ABSTRACT

Bone is one of the most preferred sites of metastasis in lung cancer. Currently, bisphosphonates and denosumab are major agents for controlling tumor-associated skeletal-related events (SREs). However, both bisphosphonates and denosumab significantly increase the risk for jaw osteonecrosis. Statins, 3-hydroxy-3-methylglutaryl coenzyme A (HMG-CoA) reductase inhibitors and the most frequently prescribed cholesterol-lowering agents, have been reported to inhibit tumor progression and induce autophagy in cancer cells. However, the effects of statin and role of autophagy by statin on bone metastasis are unknown. In this study, we report that fluvastatin effectively prevented lung adenocarcinoma bone metastasis in a nude mouse model. We further reveal that fluvastatin-induced anti-bone metastatic property was largely dependent on its ability to induce autophagy in lung adenocarcinoma cells. *Atg5* or *Atg7* deletion, or 3-methyadenine (3-MA) or Bafilomycin A1 (Baf A1) treatment prevented the fluvastatin-induced suppression of bone metastasis. Furthermore, we reveal that fluvastatin stimulation increased the nuclear p53 expression, and fluvastatin-induced autophagy and anti-bone metastatic activity were mostly dependent on p53.

1. Introduction

Lung cancer is one of the most common cancers worldwide (Siegel et al., 2011; Kuo et al., 2013). Metastasis, a critical step in cancer progression, indicates a more advanced cancer stage and poorer prognosis, and bone is a frequently preferred site of metastasis for lung cancer. Around 30–40% of patients with advanced lung cancer may develop bone metastasis leading to a dramatic increase in mortality and rapid reduction in quality of life (Rove and Crawford, 2009).

For patients with bone metastases, current treatments are designed to decrease tumor burden, prevent further progression and metastasis and inhibit tumor-associated skeletal-related events (SREs), such as pathologic fracture and spinal cord compression. Individual lesions can be surgically excised or irradiated either before or after the surgery (Suva et al., 2011). Moreover, bisphosphonates are most frequently used agents for cancer patients with bone metastases. Bisphosphonates, synthetic analogs of pyrophosphate, bind to hydroxyapatite and trigger apoptosis in osteoclasts after internalization (Lopez-Olivo et al., 2012). Denosumab, a fully human anti-RANKL monoclonal antibody, is an FDA-approved agent (2010) for the prevention of SREs in patients with solid tumors and bone metastases. Compared with bisphosphonates, denosumab may longer delay the onset of a first SRE (Scagliotti et al., 2012; Fizazi et al., 2011). However, the worst side effect of either treatment is significant increase in the risk of osteonecrosis in the jaw. Other side effects may include pyrexia, joint and muscle pain, increased risk of infections, such as cellulitis and hypocalcemia (Taylor et al., 2010; McLeod et al., 2012; Bamias et al., 2005). These side effects, especially the risk for jaw osteonecrosis, greatly restrict the use of

Abbreviations: SREs, skeletal-related events; HMG-CoA, 3-hydroxy-3-methylglutaryl coenzyme A; 3-MA, 3-methyadenine; Baf A1, Bafilomycin A1; MICA, MHC class I chain-related protein A; CQ, chloroquine; PFTα, pifithrin-α; ACC, acetyl-CoA carboxylase; ECM, extracellular matrix; BLI, bioluminescence imaging.

* Corresponding author.
** Corresponding author at: Department of Biochemistry and Molecular Biology, Medical School, Southeast University, Nanjing, Jiangsu 210009, China.
E-mail addresses: yangzuozhang@163.com (Z. Yang), suzhenyi999@163.com (Z. Su).
[1] These authors contributed equally to this work and should be considered as co-first authors.

http://dx.doi.org/10.1016/j.ebiom.2017.04.017

these therapeutic agents to control bone metastasis. Therefore, there is an urgent need to develop novel anti-bone metastasis agents with high efficacy and minimal side effects.

Statins, 3-hydroxy-3-methylglutaryl coenzyme A (HMG-CoA) reductase inhibitors, include lovastatin, simvastatin, mevastatin, fluvastatin, pravastatin, atorvastatin, rosuvastatin and cerivastatin. Statins have been widely used for lowering cholesterol, but recent research reveal other roles, such as anti-inflammation, immunomodulation, neuroprotection and antitumor effects (Zhang et al., 2013).

During the last decade, the role of statins in cancer prevention or therapy has been controversial, but accumulating evidence based on retrospective analyses support that statins could be beneficial to patients with certain types of tumors (Nielsen et al., 2012; Singh et al., 2013; Hamilton et al., 2014). In addition, numerous experimental studies have revealed that statins have a role in inhibiting tumor growth and metastasis (Campbell et al., 2006; Clendening and Penn, 2012; Hindler et al., 2006). However, the underlying mechanisms are complex, and the working hypothesis can be divided into Rho GTPase dependent and independent mechanisms. Rho GTPases are considered to be important signaling molecules that drive tumor growth and metastasis. Statins may inhibit Rho GTPase activation by interfering with mevalonate pathway and Rho geranylgeranylation, a key posttranslational modification for Rho GTPase biological activities (Collisson et al., 2003; Kusama et al., 2001; Tsubaki et al., 2015). Furthermore, statins involve the innate immune response against human metastatic melanoma cells by inducing MHC class I Chain-related protein A (MICA) membrane expression. As a result, independent of Ras and Rho GTPase signaling pathways, melanoma cells are more sensitive to lysis by NK cells (Pich et al., 2013). In addition, simvastatin may prevent triple-negative breast cancer metastasis via regulation of FOXO3a (Wolfe et al., 2015).

Although statins may trigger autophagy in a few cancer cells through inhibition of geranylgeranylation (Araki et al., 2012; Yang et al., 2010; Parikh et al., 2010), whether statin-induced autophagy plays a role in promotion or suppression of cancer metastasis is largely unknown. Only few in vitro studies showed that inhibition of autophagy may enhance statin-induced apoptosis or cytotoxicity in some cancer cell lines (Yang et al., 2010; Misirkic et al., 2012; Kang et al., 2014). The role of autophagy in tumorigenesis and progression is quite complicated, because induction of autophagy could either accelerate the tumor progression or suppression (Zhang et al., 2013; Su et al., 2015a). Many studies emphasize cancer stages, cancer types and tumor microenvironments as the determining factors. In our current study, we validate that statins prevent lung adenocarcinoma bone metastasis though triggering autophagy. Moreover, we propose a mechanism by which autophagy serves a positive role in suppression of cancer bone metastasis.

p53, the most well-known tumor suppressor, serves a critical role in safeguarding the integrity of the genome. After activation by intracellular stresses, such as DNA damage, hypoxia and oncogene activation, p53 initiates a series of cell events including apoptosis, cell cycle arrest and DNA repair to suppress tumorigenesis (Jin, 2005). In recent years, p53 has been revealed to play an important role in either inducing or suppressing autophagy depending on its subcellular localization. Specifically, nuclear p53 acts as a transcription factor to activate a series of pro-autophagic genes; cytoplasmic p53 serves a role in repressing autophagy via unclear mechanisms (Maiuri et al., 2010; Tasdemir et al., 2008). In this study, we investigate the involvement of p53 in both fluvastatin-induced autophagy and suppression of lung adenocarcinoma bone metastasis and determine the signaling pathway bridging p53 to autophagy.

2. Materials & Methods

2.1. Reagents

Nuclear and Cytoplasmic Protein Extraction Kit (Beyotime Biotech, China); Lipofectmin 2000 (Invitrogen, USA); Entranster™-in vivo transfection reagent (Engreen Biosystem, China); pifithrin-α (Sigma, USA); fluvastatin (Novartis Pharma, Switzerland); 3-methyadenine (Sigma, USA); Bafilomycin A1 (Santa Cruz, CA, USA), chloroquine (MedChemExpress, USA), denosumab (Prolia, Amgen Inc., USA); mouse-anti-AMPKα1/2 (sc-74461, Santa Cruz, USA); rabbit-anti-pAMPKα1/2 (Thr 172) (sc-33524, Santa Cruz, USA); rabbit-anti-ACCα (sc-30212, Santa Cruz); rabbit-anti-ACCα (sc-271965, Santa Cruz); mouse-anti-PTEN (sc-7974, Santa Cruz); rabbit-anti-AKT (sc-8312, Santa Cruz); rabbit-anti-pAKT (Ser 473) (sc-33437, Santa Cruz); rabbit-anti-Histone H3 (sc-10809, Santa Cruz); mouse-anti-p53 (sc-126, Santa Cruz); rabbit-anti-LC3 (sc-28266, Santa Cruz); rabbit-anti-mTOR (sc-8319, Santa Cruz); rabbit-anti-mTOR (Ser 2448) (sc-101738, Santa Cruz); mouse-anti-β-Actin (sc-47778, Santa Cruz).

2.2. Cells

293 T cells and the human lung adenocarcinoma cell line A549 were obtained from the ATCC and cultured with DMEM (Invitrogen, USA) supplemented with 10% fetal bovine serum (Hyclone, USA). Human lung adenocarcinoma cell line SPC-A-1 was purchased from the Cell Resource Centre of Shanghai Institutes for Biological Sciences of the Chinese Academy of Sciences and cultured with RPMI 1640 medium (Invitrogen, USA) supplemented with 10% fetal bovine serum. Luciferase-expressing SPC-A-1 cells were established in our lab by a stable transfection with pCMV-G Luc 2 plasmid (New England Biolabs, USA). *Atg5*$^{-/-}$ and *Atg7*$^{-/-}$ SPC-A-1 cells were established by CRISPR/Cas9 system (Inovogen, Beijing, China). Exon 2 of *Atg5* and exon 1 of *Atg7* were selected for design of guide RNA. Guide RNA sequences: Atg5: 5′-TGCTTCGAGATGTGTGGTT-3′; Atg7: 5′-AAGCTGAACGAGTATCGGC-3′.

2.3. Wound Healing Assay

Briefly, after seeding A549 or SPC-A-1 cells in 12-well plates, media was changed to 0.1% FBS DMEM before scratching. Scratch wound was generated with a 10 μl pipette tip, and then cells were incubated with 10 μM fluvastatin or combined with other drugs at different time points. Photographs were taken at indicated time points. The percentage of wound healing was calculated using the Image J software. Wound healing rate (%) = (initial wound area − non-healing area)/initial wound area.

2.4. Matrigel Invasion Assay

The Matrigel invasion assay was done using the BD Biocoat Matrigel Invasion Chamber (pore size: 8 μm, 24-well; BD Biosciences) and following the manufacturer's protocol. Cells (5×10^4) were plated in the upper chamber in serum-free medium with 10 μM fluvastatin or other drugs. The bottom chamber contained medium with 10% FBS. After indicated times, the cells that had invaded through the membrane to the lower surface were fixed, stained with 0.1% Crystal Violet and counted by microscopy.

2.5. Bioluminescence Imaging (BLI)

Mice were inoculated with 5×10^6 luciferase-transfected SPC-A-1 cells and then treated with different drugs for 3 weeks. At the end of treatment, mice were injected (i.p.) with 100 μl of the D-luciferin solution (150 mg/kg) (Gold Biotechnology, St. Louis, MO). During the image acquisition, mice were anesthetized with 50 mg/kg pentobarbital sodium (i.p.) and then imaged in a dorsal position using the Xenogen IVIS Spectrum system (Caliper Life Sciences, USA). Signal intensity in both left and right hind limbs was quantified as photons flux (photons/s/cm^2/sr) using Living Image software 4.2 (Caliper Life Sciences) as described previously (Hu et al., 2011).

2.6. In vivo Lung Adenocarcinoma Bone Metastasis Experiments

The female BALB/c nude mice (4–6 weeks, purchased from Beijing Vital River Ltd., China) were injected with 5×10^6 SPC-A-1-luc cells (in some experiments, *Atg5*$^{-/-}$ or *Atg7*$^{-/-}$ SPC-A-1 cells were used) via the heart's left ventricle. One week later, mice were divided into different groups ($n = 6$) and injected (i.p.) with normal saline or different drugs (e.g., fluvastatin, 50 mg/kg; denosumab, 120 mg/kg; fluvastatin + 3-MA (10 mg/kg/d); fluvastatin + Baf A1 (1 mg/kg); fluvastatin + PFTα (2 mg/kg)) every day for 3 weeks. At the end of treatment, mice were subjected to X-ray radiography, and tissues were fixed and embedded in paraffin for histological analysis. For in vivo p53 knockdown experiment, mice were injected (i.v.) with p53-shRNA plasmid or negative control shRNA plasmid carried with Entranster™-in vivo transfection reagent every seven days to sustain the knockdown effect in vivo. These mice were inoculated with luciferase-transfected SPC-A-1 cells and then injected with 50 mg/kg fluvastatin every day for 3 weeks from the 7th day of post tumor challenge. At the end of treatment, mice were subjected to X-ray radiography, and tissues were fixed and embedded in paraffin for histological analysis and immunohistochemistry staining. For survival curve study, mice ($n = 20$) were injected (i.v.) with p53-shRNA or negative control shRNA plasmid every seven days. After one week of post tumor challenge, mice received 50 mg/kg fluvastatin every two day for 20 weeks. The statistical difference of survival curves was determined by the Log-rank (Mantel-Cox) test.

2.7. X-ray Analysis and Micro-CT

At the end of drugs treatment, mice were anesthetized and subjected to X-ray radiography in the prone position. Osteolytic lesions were identified as demarcated radiolucent lesions on radiographs. X-ray lesion area was determined from femurs and tibia and quantified using the Image J software. For some experiments, we detected and evaluated the bone lesions by micro-CT via calculating the bone volume/total volume (BV/TV), trabecular number (Tb.N), trabecular thickness (Tb.Th) and trabecular separation (Tb.Sp).

2.8. Hematoxylin and eosin (H&E) staining and immunohistochemistry staining

At the end of experiment, mice were euthanized, and hind limbs were collected and fixed in 10% neutral buffered formalin for 48 h, followed by decalcification in 10% EDTA for 2 weeks. Next, bone tissues were embedded in paraffin wax for sectioning (thickness, 3.5 μm) and stained with H&E. Bone sections were also dewaxed and subjected to immunohistochemistry staining using LC3 antibody. LC3 expression was scored as following: 0, no staining; 1, weak staining; 2, moderate staining; and 3, strong staining.

2.9. Electron Microscope Imaging

SPC-A-1 and A549 cells, treated with 10 μM fluvastatin for 24 h, were collected and fixed with 2.5% glutaraldehyde (MP Biomedicals, USA). Ultrathin sections of samples were stained with uranyl acetate and lead citrate, and the autophagosomes were observed and captured by Transmission Electron Microscopy (TEM) (JEM-1011 electron microscope, Hitachi, Japan).

2.10. LC3 Puncta Analysis

1×10^5 SPC-A-1 and A549 cells were seeded in a six-well plate and transfected with GFP-LC3 plasmid (Addgene, USA) using Lipofectamine 2000 reagent (Invitrogen, USA). After eighteen-hour transfection, cells were incubated with different drugs or transfected with siRNAs for indicated times. GFP-LC3 puncta were detected using a fluorescence microscope (DMI6000B, Leica, Germany). To quantify the average number of GFP-LC3 puncta per cell, 200–300 cells in four random fields were counted.

In some experiments, we also transfected SPC-A-1 cells with mCherry-GFP-LC3 plasmid (Addgene) to track autophagy (Castillo et al., 2013). The GFP fluorescence is sensitive to acidic conditions of the lysosome and will be attenuated when autophagosome fuses with lysosome. Yellow LC3 puncta (colocalization of GFP and mCherry fluorescence) indicates that the mCherry-GFP-LC3 protein is on the phagophore or within the autophagosome; red puncta (strong mCherry signal but weak GFP signal) indicates that the protein is within the autolysosome.

2.11. SiRNA Transfection and Lentivirus-based Gene Knockdown

SPC-A-1 cells were seeded and transfected with 100 nM negative control (NC) siRNA or p53 siRNA using Lipofectamine 2000 reagent (Invitrogen). After twelve-hour transfection, cells were incubated with fluvastatin for another 24 h. The sequence of human p53 siRNA is 5′-CGA TATTGA ACA ATG GTT CAC TGA A-3′. To get a better knockdown efficiency, we also used lentivirus-based p53 knockdown in some in vitro experiments. p53 shRNA (the core sequence is same as above) were cloned into pLVX-shRNA1 (Clontech), and high-titer lentiviral stocks were generated by co-transfecting packaging vectors into 293 T cells as described previously (Rocco et al., 2006). Viral supernatants were collected 48 h post transfection and used for SPC-A-1 infection. For in vivo experiments, we used p53-shRNA plasmid carried with Entranster™-in vivo transfection reagent.

2.12. Statistical Analysis

Data were expressed as means and SD and analyzed by two-tailed t-tests and the Log-rank (Mantel-Cox) test (for survival curve analysis). A p-value < 0.05 was considered statistically significant.

3. Results

First, we examined the role of fluvastatin in the regulation of lung adenocarcinoma cell migration. As shown in Fig. 1A, fluvastatin significantly delayed the wound-healing time in A549 and SPC-A-1 cells compared with the control. Consistent with the wound-healing result, Matrigel invasive assay revealed that fluvastatin strongly prevented the invasion of adenocarcinoma cells (Fig. 1B). To further investigate the anti-metastatic role of fluvastatin in vivo, we established a lung adenocarcinoma bone metastatic model in nude mice by injecting SPC-A-1 cells into the heart's left ventricle. Bioluminescence imaging showed that tumor dissemination was effectively blocked by fluvastatin treatment, and overall, this treatment had greater efficacy than the positive anti-bone metastatic drug denosumab (Fig. 1C and D). Furthermore, X-ray images also showed reduced lesions and damage on bones after the fluvastatin treatment (Fig. 1C and E). H&E staining in Fig. 1C illustrated deep purple tumor cells with irregularly shaped nucleus occupying the bone marrow cavity and replacing normal bone marrow cells in sections from untreated mice. Moreover, metastatic lung adenocarcinoma cells caused abrupt lysis of long bones, reduction in trabecular bone density and gradual destruction of cortical bone. Bone sections from denosumab-treated mice showed a mixture of tumor and bone marrow cells in tibia but the tumor cells were restricted to the cortical bone. Fluvastatin treatment resulted in a complete reduction in the number of tumor cells in tibia and lesions of bone structure. These results suggest an inhibitory role of fluvastatin in lung adenocarcinoma metastasis, specifically in bone metastasis.

Since fluvastatin has a role in the suppression of lung adenocarcinoma bone metastasis, we subsequently explored the underlying mechanisms. We found that fluvastatin can induce autophagy in both SPC-A-1 and A549 cells. Electron microscope images showed an increased

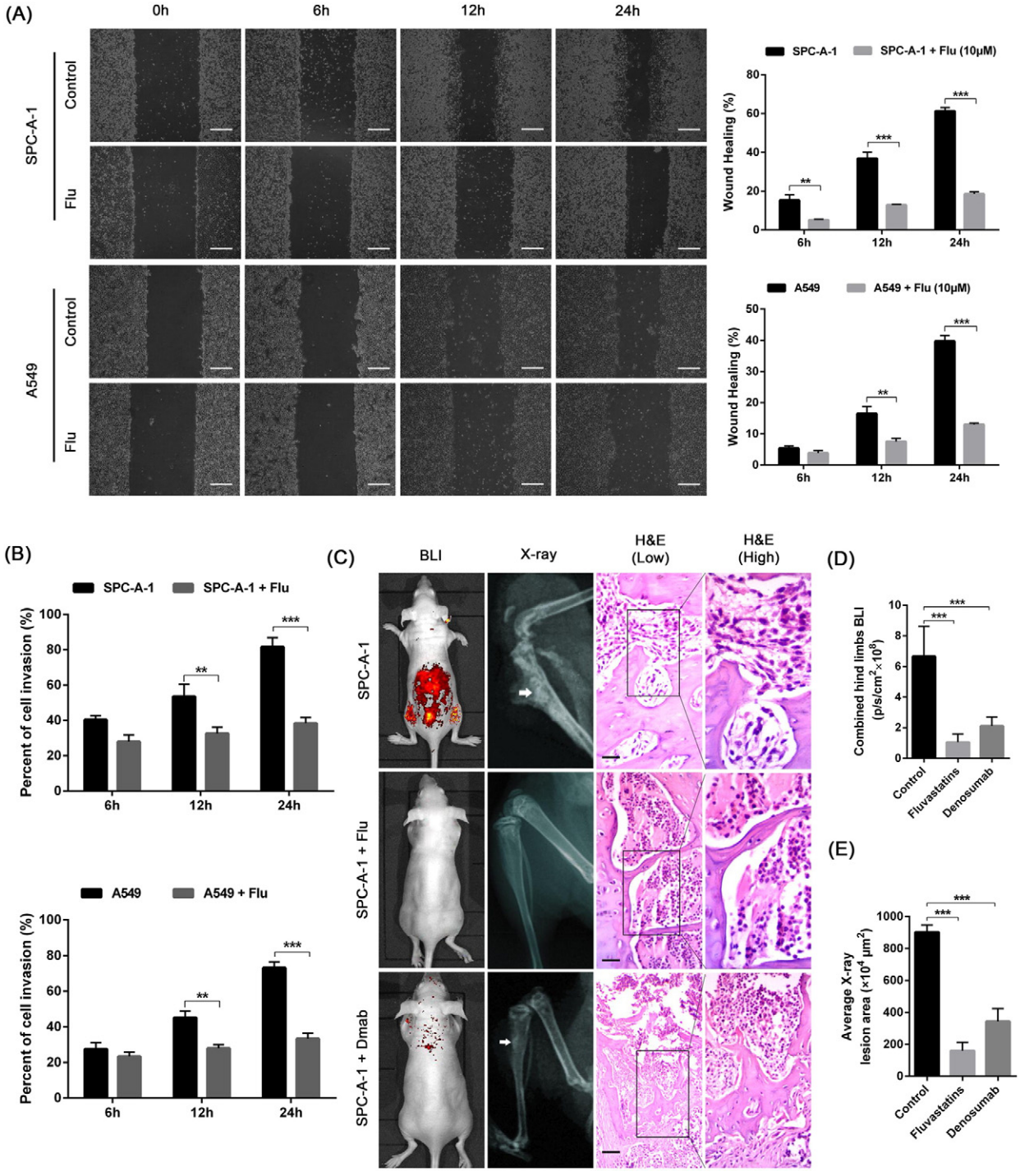

Fig. 1. The anti-metastatic role of fluvastatin in vitro and in vivo. (A) The effect of fluvastatin (Flu) on migration of SPC-A-1 and A549. Migration was measured by wound-healing assay. Left graph, representative images of different post-wound time points (0, 6, 12, or 24 h); right graph, quantification of wound-healing data. Wound healing rate (%) = (initial wound area − non-healing area)/initial wound area. Scale bar, 200 μm. (B) Matrigel invasive assay of SPC-A-1 and A549 cells (6–24 h). Migratory cells were counted in 10 non-overlapping areas using Stereologer. Flu, 10 μM. (C) Representative images of anti-metastatic role of fluvastatin in vivo. Mice ($n = 6$ per group) were injected with 5×10^6 luciferase-transfected SPC-A-1 cells. On the 7th day, mice were injected with Flu (50 mg/kg), denosumab (Dmab, 120 mg/kg) or normal saline every day for 3 weeks. Tumor metastases are shown by bioluminescence imaging (BLI) (left), and bone lesions of hind limbs were detected by X-ray (middle) and Hematoxylin and Eosin (H&E) staining (right). Tumor cells in H&E staining images can be identified by deep purple color and irregular nuclear shape. Bone lesions are shown with white arrows. Scale bar, 50 μm. (D) Quantification of X-ray lesion areas ($n = 6$ per group). (E) Quantification of BLI data. Bioluminescence was measured by mean photon counts per second per cm^2 ($n = 6$ per group). $^*p < 0.05$ (compared with the control groups).

autophagosomes upon fluvastatin stimulation (Fig. 2A). Furthermore, after the fluvastatin induction, a larger number of GFP-LC3 puncta formed indicating the presence of autophagosomes (Fig. 2B). These data were in accordance with the dose-dependent increase of LC3IIexpression upon fluvastatin stimulation as shown in Fig. 2C.

Another tool to track autophagy is using the tandem monomeric mCherry-GFP-LC3 tagged protein. The GFP fluorescent signal is very sensitive to acidic conditions of the lysosome lumen and easily quenched, while the mCherry fluorescence is more stable in the lysosome. Therefore, colocalization of GFP and mCherry fluorescence

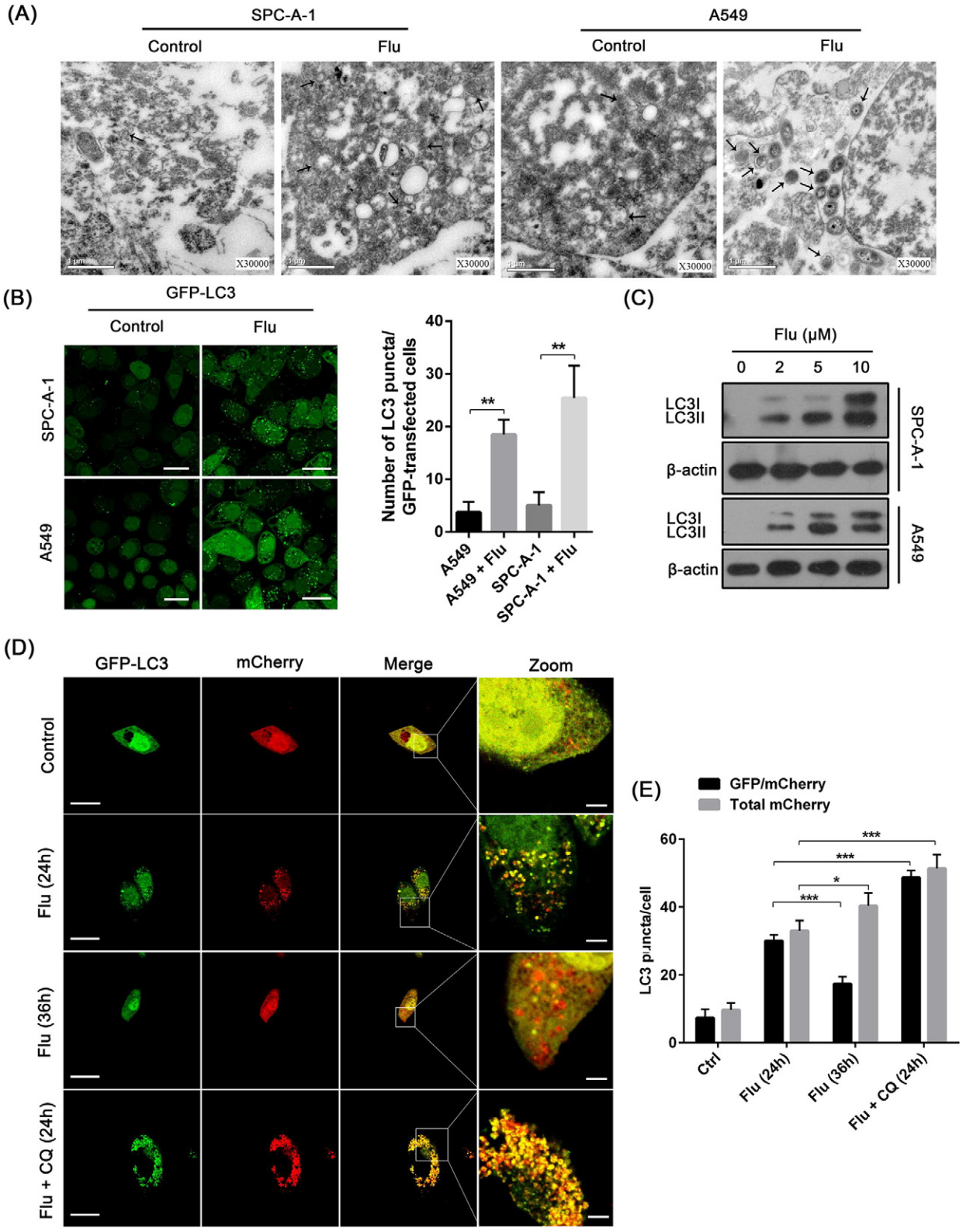

Fig. 2. Fluvastatin induces autophagy in lung adenocarcinoma cells. (A) Autophagosome detection by electron microscope. SPC-A-1 and A549 cells treated with 10 μM Flu for 24 h. Black arrows indicate autophagosomes. Scale bar, 1 μm. (B) GFP-LC3 puncta analysis by fluorescence microscopy. Left, representative images of GFP-LC3 puncta upon Flu treatment (10 μM for 24 h); right, quantification of average number of GFP-LC3 puncta per cell. Scale bar, 10 μm. (C) Western blot analysis of LC3 expression upon Flu stimulation (0–10 μM). (D) mCherry-GFP-LC3 puncta analysis in SPC-A-1 cells. Cells were transfected with mCherry-GFP-LC3 plasmid and incubated for 6 h. Next, cells were pretreated with or without CQ (50 μM) for 1 h followed by stimulation of 5 μM Flu for 24 h or 36 h. Scale bar, 10 μm and 2 μm (magnified graph). (E) Quantification of GFP and yellow LC3 puncta. $^{*}p < 0.05$, $^{**}p < 0.01$, $^{***}p < 0.001$.

(yellow puncta) indicates that the tandem protein is on the phagophore or within the autophagosome; strong mCherry signal but weak/no GFP signal (red puncta) indicates that the protein is within the autolysosome. As shown in Fig. 2D, stimulation with fluvastatin showed a strong increase in yellow LC3 puncta at 24 h and decrease from 36 h, suggesting the formation of autophagosome and subsequent fusion with lysosome. The lysosomal inhibitor chloroquine (CQ) raised the lysosomal pH and increased the autophagic flux (more GFP and mCherry puncta) (Fig. 2D). The quantification of yellow and red LC3 puncta is shown in Fig. 2E. In accordance with LC3 fluorescence results, fluvastatin induced strong LC3-IIexpression between 12 and 24 h, but the expression decreased from 24 h; pretreatment with CQ delayed

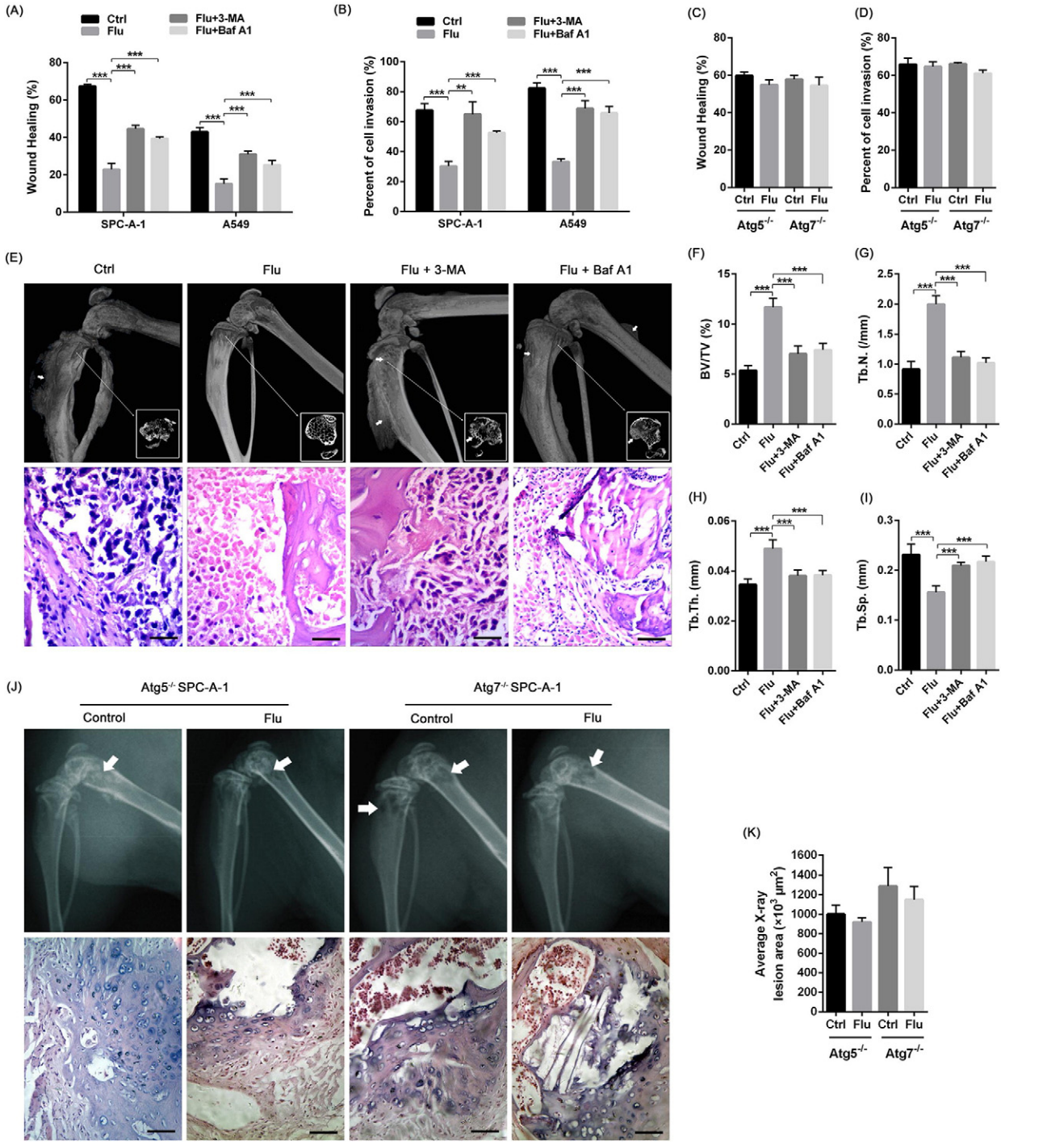

Fig. 3. The anti-metastatic role of fluvastatin is dependent on autophagy. (A) The effect of autophagy inhibitors on wound-healing of SPC-A-1 and A549. 3-MA, 3-methyadenine (10 mM); Baf A1, Bafilomycin A1 (100 nM); PFTα, pifithrin-α (20 μM). Duration of each drug treatment, 24 h. (B) The effect of autophagy inhibitors on invasion of SPC-A-1 and A549 cells. Invasive ability was evaluated by calculating the percentage of cells invaded through Matrigel and Transwell membranes. Duration of each drug treatment, 24 h. (C-D) The effect of Flu on wound-healing and invasion of *Atg5*$^{-/-}$ and *Atg7*$^{-/-}$ SPC-A-1 cells. (E) Micro-CT assay and H&E staining of bone lesions. Tumor cells in H&E staining images can be identified by deep purple color and irregular nuclear shape. Mice ($n = 6$ per group) were inoculated with 5×10^6 SPC-A-1 lung adenocarcinoma cells for seven days and treated with Flu (50 mg/kg/d), Flu + 3-MA (10 mg/kg/d) and Flu + Baf A1 (1 mg/kg/d) for 3 weeks. White arrows indicate osteolytic bone lesions. Scale bar, 50 μm. (F–I) Quantitative analysis of bone damages shown in micro-CT images. F, BV/TV (bone volume/total volume); G, Tb.N (trabecular number); H, Tb.Th (trabecular thickness); I, Tb.Sp (trabecular separation). (J) X-ray assay and H&E staining of bone lesions of *Atg5*$^{-/-}$ and *Atg7*$^{-/-}$ SPC-A-1 cells in presence or absence of Flu (50 mg/kg/d). $n = 6$ per group. Scale bar, 50 μm. (K) The quantification of lesion area in X-ray images. $^*p < 0.05$, $^{**}p < 0.01$, $^{***}p < 0.001$.

the degradation of LC3II (Fig. S1A). Next, we established autophagy-defective SPC-A-1 cells by deleting *Atg5* or *Atg7* gene using CRISPR/Cas9 system and there was no LC3II induction in response to fluvastatin or rapamycin in these cells. The knockout effect of *Atg5* or *Atg7* was validated by Western blot (Fig. S1B, C). Taken together, these findings demonstrate that fluvastatin induces autophagy in lung adenocarcinoma cells in a time and dose dependent manner.

Since fluvastatin can both trigger autophagy and inhibit lung adenocarcinoma bone metastasis, we next investigated the causal relationship between induction of autophagy and prevention of lung adenocarcinoma bone metastasis. We first determined the effect of fluvastatin on lung adenocarcinoma cell migration and invasion in vitro. Wound healing experiment showed that the fluvastatin-induced healing inhibition was greatly attenuated by autophagy inhibitor 3-methyadenine (3-MA) or Bafilomycin A1 (Baf A1) in either A549 or SPC-A-1 cells (Fig. 3A). In addition, 3-MA or Baf A1 also markedly blocked fluvastatin-induced anti-invasive effect in Matrigel invasion experiment (Fig. 3B). Results were similar in $Atg5^{-/-}$ or $Atg7^{-/-}$ SPC-A-1 cells, in which fluvastatin lost the ability to inhibit the migration and invasion of SPC-A-1 cells (Fig. 3C, D). These findings suggest the critical role of autophagy in fluvastatin-induced inhibition of migration and invasion in lung adenocarcinoma cells.

We next investigated the function of autophagy in fluvastatin-induced suppression of bone metastasis in vivo. In accordance with the in vitro data, 3-MA or Baf A1 treatment also reversed the protective effect of fluvastatin on bone lesions. As shown in Fig. 3E, bone sections from untreated mice showed a large number of tumor cells in tibia. Bone sections from fluvastatin-treated mice revealed tumor cell reduction. However, pretreatment with 3-MA and Baf A1 inhibited the protective effect of fluvastatin on tumor invasion and bone destruction. Micro-CT images showed alleviated bone damage from fluvastatin treatment with significantly increased the bone volume/total volume (BV/TV), trabecular number (Tb.N) and trabecular thickness (Tb.Th), but decreased the trabecular separation (Tb.Sp); inhibition of autophagy by 3-MA or Baf A1 blocked the fluvastatin-induced anti-bone metastatic function (Fig. 3F–I). To further validate the essential role of autophagy in this process, we used autophagy defective cells, $Atg5^{-/-}$ or $Atg7^{-/-}$ SPC-A-1 to establish lung adenocarcinoma bone metastasis to show that fluvastatin lost the protective effect on bone metastasis; X-ray imaging and H&E staining confirmed this finding (Fig. 3J, K). Bone sections from mice inoculated with the $Atg5^{-/-}$ or $Atg7^{-/-}$ SPC-A-1 cells displayed remarkable tumor-induced osteolysis, and fluvastatin lost the ability to protect the integrity of bones in autophagy-defective tumors (Fig. 3J). The quantification of lesion area is

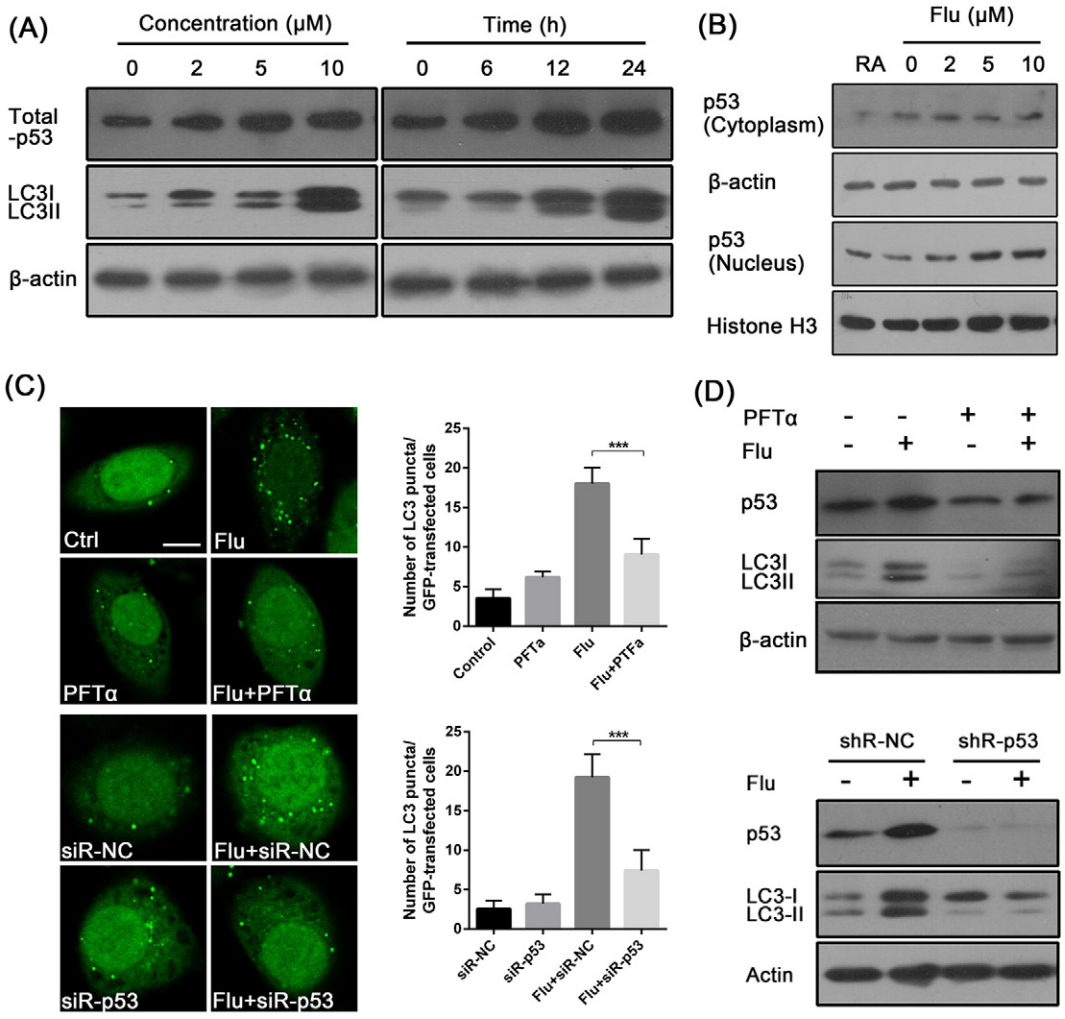

Fig. 4. Fluvastatin-induced autophagy is dependent on p53. (A) Dose- and time-dependent induction of total p53 by fluvastatin in SPC-A-1. (B) Nuclear and cytosolic p53 expression upon Flu stimulation (0–10 μM). RA, rapamycin (100 nM). (C) The effect of p53 inhibitor and p53 knockdown on GFP-LC3 puncta formation. SPC-A-1 cells were transfected with GFP-LC3 plasmids for 18 h and then pretreated with 20 μM PFTα for 2 h or infected with negative control siRNA (siR-NC) or p53 siRNA (siR-p53), followed by incubation with 10 μM Flu for an additional 24 h. Right panels, quantitative analysis of the average number of LC3 puncta per cell. Scale bar, 10 μm. (D) Western blot analysis of autophagy marker LC3 expression upon Flu stimulation in presence or absence of PFTα or with or without knockdown of p53. $^{*}p < 0.05$, $^{**}p < 0.01$, $^{***}p < 0.001$.

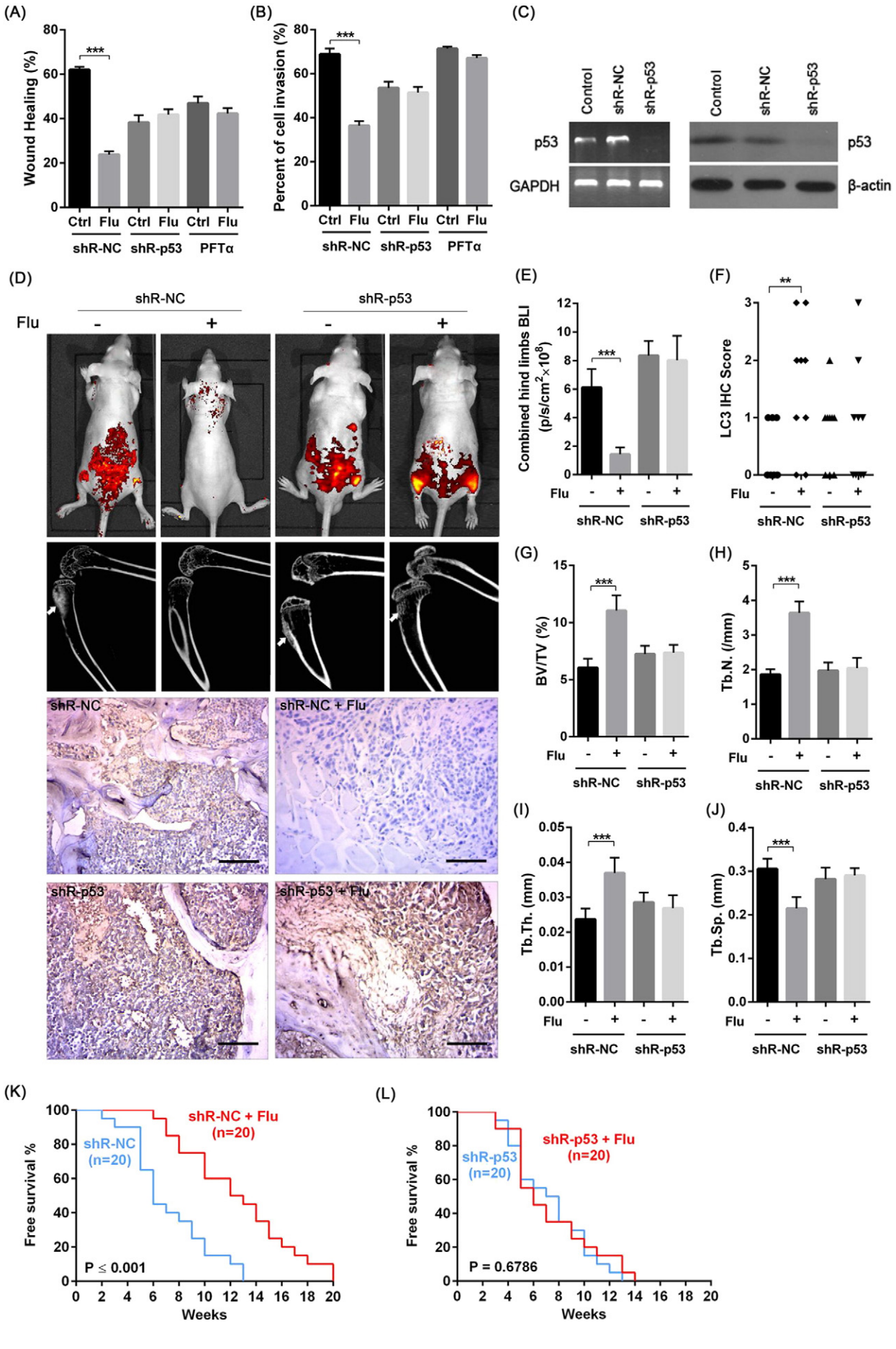
(A)
Wound Healing (%)
***
Ctrl Flu Ctrl Flu Ctrl Flu
shR-NC shR-p53 PFTα
(B)
Percent of cell invasion (%)
***
Ctrl Flu Ctrl Flu Ctrl Flu
shR-NC shR-p53 PFTα
(C)
Control shR-NC shR-p53 Control shR-NC shR-p53
p53
GAPDH
p53
β-actin
(D)
shR-NC shR-p53
Flu - + - +
shR-NC
shR-NC + Flu
shR-p53
shR-p53 + Flu
(E)
Combined hind limbs BLI (p/s/cm²×10⁸)
***
Flu - + - +
shR-NC shR-p53
(F)
**
LC3 IHC Score
Flu - + - +
shR-NC shR-p53
(G)
BV/TV (%)
***
Flu - + - +
shR-NC shR-p53
(H)
Tb.N. (/mm)
***
Flu - + - +
shR-NC shR-p53
(I)
Tb.Th. (mm)
***
Flu - + - +
shR-NC shR-p53
(J)
Tb.Sp. (mm)
***
Flu - + - +
shR-NC shR-p53
(K)
Free survival %
shR-NC (n=20)
shR-NC + Flu (n=20)
P ≤ 0.001
Weeks
(L)
Free survival %
shR-p53 (n=20)
shR-p53 + Flu (n=20)
P = 0.6786
Weeks

shown in Fig. 3K. These data support that the anti-metastatic function of fluvastatin in vitro and in vivo is greatly mediated by autophagy in lung adenocarcinoma cells.

Since p53 is reported to be a critical component in autophagy pathways, we studied the role of p53 in fluvastatin-induced autophagy. We found that fluvastatin induced total p53 expression in a dose and time dependent manner (Fig. 4A). Further study showed fluvastatin did not significantly increase the protein level of cytosolic p53, but increase the nuclear p53 level (Fig. 4B). As shown in Fig. 4C, fewer numbers of GFP-LC3 puncta were formed upon fluvastatin treatment in the presence of p53 inhibitor pifithrin-α (PFTα). This was in agreement with the Western blot results (Fig. 4D upper panel) showing the inhibition of LC3II formation by PFTα. Similarly, p53 knockdown in SPC-A-1 cells also blocked fluvastatin-induced LC3 puncta accumulation (Fig. 4C), as well as LC3II expression (Fig. 4D lower panel). These findings demonstrate that p53 is a key mediator that bridges fluvastatin to autophagy.

Next, we investigated whether p53 plays an important role in fluvastatin-induced anti-metastatic property in vitro and in vivo. Wound healing experiment showed that the fluvastatin-induced healing inhibition was greatly attenuated by either p53 knockdown or PFTα in SPC-A-1 cells (Fig. 5A). In addition, p53 knockdown or PFTα also markedly blocked fluvastatin-induced anti-invasive effect in Matrigel invasion experiment (Fig. 5B).

To further confirm the pivotal role of p53 in fluvastatin-induced anti-bone metastatic activity and survival, we intravenously injected p53 shRNA or negative control shRNA plasmids into mice every week to establish an in vivo p53 knockdown model. As shown in Fig. 5C, the p53 mRNA and protein levels were effectively inhibited in tumor nodes of lung tissue after the in vivo injection of p53 shRNA. As expected, bioluminescence imaging indicated that fluvastatin markedly prevented the dissemination of cancer cells to other tissues especially to the skeleton in the control but not in the p53 knockdown model (Fig. 5D top, and E). Similarly, micro-CT analysis also confirmed that with p53 expression attenuation, fluvastatin did not block the bone damage (BV/TV, Tb.N and Tb.Th decreased and Tb.Sp increased) caused by lung adenocarcinoma cells (Fig. 5D middle and G–J). In accordance with the impaired anti-bone metastatic activity, autophagic level of cancer cells in bone lesion regions was also decreased by p53 knockdown (Fig. Fig. 5D bottom and F). Notably, a 20-week survival follow-up strongly supported that long-term treatment with fluvastatin greatly extended the longevity of normal mice inoculated with SPC-A-1 lung adenocarcinoma cells (Fig. 5K). However, fluvastatin had no protective effect in prolonging the survival when p53 was knockdown in vivo (Fig. 5L). These findings suggest that anti-bone metastatic property and survival-extending ability of fluvastatin are highly dependent on the p53 level in tumors.

We next examined the signaling pathway in activation of autophagy employed by fluvastatin. Fluvastatin markedly induced phosphorylation of AMPK and acetyl-CoA carboxylase (ACC) (Fig. 6A). ACC, a downstream molecule of AMPK, can be phosphorylated and inactivated by AMPK and serves as a marker for AMPK activation. In contrast, fluvastatin neither changed the expression of PTEN nor the phosphorylation of AKT, which is another pathway for autophagy induction (Su et al., 2015b). To further clarify the role of p53 in fluvastatin-induced autophagic pathway, we knockdown p53 by lentivirus-based shRNA or inhibited p53 by PFTα. We found that fluvastatin-induced AMPK phosphorylation and mTOR (Ser-2448) dephosphorylation were mostly blocked showing a p53-dependent pattern (Fig. 6B). It was reported that the phosphorylation of Ser-2448 was dependent on mTOR kinase activity (Chiang and Abraham, 2005), so the reduced phosphorylation of mTOR Ser-2448 is marker for mTOR inhibition and activation of autophagy. These results imply that fluvastatin-triggered autophagy is mediated by the p53-AMPK-mTOR signaling pathway.

4. Discussion

It is widely known that wild-type p53 protein is a tumor suppressor, whereas mutant p53 proteins can actively contribute to tumorigenesis. p53 mutations have been revealed to be present in numerous human tumors (Muller and Vousden, 2013). Recently, Freed-Pastor et al. reported the significant upregulation of mutant p53 in the mevalonate pathway. Specifically, mutant p53 is recruited to sterol gene promoters partly via SREBP transcription factors and induces sterol biosynthesis of genes that increase the malignancy of breast cancers. Inhibition of mevalonate pathway by statins is sufficient to block the phenotypic effects of mutant p53 on breast tissue architecture. This study demonstrated a novel anti-tumor mechanism in which statins prevent the tumor progression by blocking the signaling pathway of mutant p53 (Freed-Pastor et al., 2012). In our study, we demonstrate the role of statins on normal, wild-type p53. Specifically, we illustrate that fluvastatin induces nuclear wild-type p53 expression activating the AMPK-mTOR-dependent autophagy in cancer cells to increase anti-bone metastatic effect. This suggests that statins can regulate both normal p53 and mutant p53 functions and contribute to a tumor suppressive effect.

Pei-Ming Yang et al. reported that atorvastatin could inhibit the growth of hepatocellular carcinoma and colorectal carcinoma cells via induction of apoptosis; inhibition of autophagy increased atorvastatin-induced cell apoptosis (Yang et al., 2010). Unlike this study looking at in vitro cell apoptosis in primary cancer cell lines, our study focuses on autophagy in bone metastasis. In fact, the role of autophagy in cancer metastasis is quite complicated (Kenific et al., 2010). Generally, induction of autophagy could either promote the tumor progression or suppression and is mostly dependent on cancer stages, cancer types and tumor microenvironment. Autophagy may exert a suppressive effect in the early stage of cancer metastasis by promoting oncogene-induced senescence, restricting tumor necrosis or inflammation and triggering autophagic cell death to reduce invasion and dissemination of cancer cells from the primary site. In addition, autophagy was reported to degrade TWIST1 to restrict epithelial-mesenchymal transition (Qiang and He, 2014). During advanced cancer stages, autophagy may accelerate metastasis by supporting extracellular matrix (ECM)-detached metastatic cell survival and inducing metastatic cells to enter dormancy if they fail to establish a contact with the ECM in the new environment. Furthermore, tumor colonization at a distant site is possible by increasing the motility of tumor cell via autophagy-induced degradation of paxillin and focal adhesion turnover (Su et al., 2015a; Peng et al., 2013; Sharifi et al., 2016). Recently, Rosenfeldt et al. reported that p53

Fig. 5. In vitro and in vivo knockdown of p53 abolishes the fluvastatin-induced anti-metastatic function. (A) The effect of p53 knockdown or p53 inhibition on wound-healing of SPC-A-1 cells in presence or absence of Flu. PFTα, 20 μM; Flu, 10 μM. (B) The effect of p53 knockdown or p53 inhibition on invasion of SPC-A-1 cells in presence or absence of Flu by Matrigel invasion assay. (C) p53 knockdown efficiency in SPC-A-1 tumor nodes by RT-PCR and Western blot. Control, without injection of shRNA plasmid. Injection dose (per mouse): 50 μg NC or p53 shRNA plasmid mixed with 100 μl EntransterTM-in vivo. (D) The impact of p53 knockdown on fluvastatin-induced inhibition of bone metastasis. Mice were injected (i.v.) with p53-shRNA plasmid or negative control (NC) shRNA plasmid every seven days to sustain the knockdown effect in vivo ($n = 9$ per group). These mice were inoculated with luciferase-transfected SPC-A-1 cells and then injected with 50 mg/kg fluvastatin every day for 3 weeks from the 7th day post tumor challenge. SPC-A-1 metastases were shown by bioluminescence imaging (BLI) (top); bone lesions of hind limbs were shown by micro-CT (middle); LC3 expression in bone lesions was examined by immunohistochemistry (IHC) staining (bottom). Scale bar, 50 μm. (E) Quantification of metastasis in bioluminescence images. Bioluminescence was measured by mean photon counts per second per cm^2. (F) Scoring of IHC results. 0: no staining; 1: weak staining; 2: moderate staining; and 3: strong staining. (G–J) Quantitative analysis of bone lesions in micro-CT images. G, BV/TV (bone volume/total volume); H, Tb.N (trabecular number); I, Tb.Th (trabecular thickness), J, Tb.Sp (trabecular separation). (K) Survival curve of negative control shRNA (NC-shRNA) treatment mice. Mice were injected with luciferase-expressed 5×10^6 SPC-A-1 cells and then treated with or without fluvastatin (50 mg/kg) every two days for 20 weeks ($n = 20$). (L) Survival curve of p53 shRNA treatment mice with or without the treatment of fluvastatin ($n = 20$). $^*p < 0.05$, $^{**}p < 0.01$, $^{***}p < 0.001$.

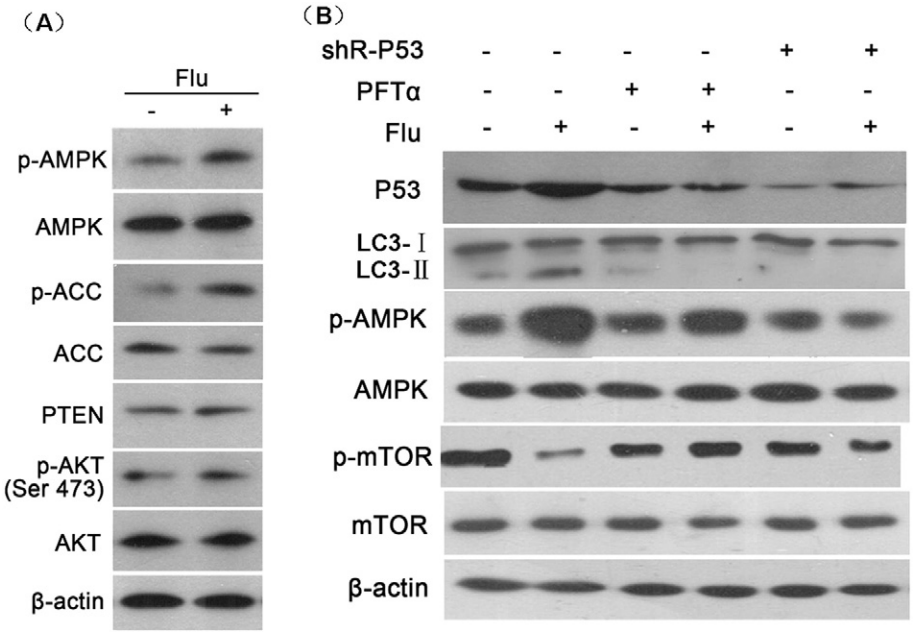

Fig. 6. Fluvastatin-induced autophagy is mediated by the p53-AMPK-mTOR pathway. (A) The effect of fluvastatin on some key components of autophagic pathway in SPC-A-1 cells. Fluvastatin, 10 μM; treatment for 24 h. ACC, acetyl-CoA carboxylase, can be phosphorylated and inactivated by AMPK. (B) The impact of p53 inhibition or knockdown on fluvastatin-induced AMPK and mTOR phosphorylation. SPC-A-1 cells were pre-incubated with 20 μM PFTα for 2 h or infected with lentivirus-based p53 shRNA for 12 h and then incubated with 10 μM fluvastatin for 24 h. After treatments, cells were lysed and subjected to Western blot analysis.

status in tumor host determined the role of autophagy in pancreatic tumor development (Rosenfeldt et al., 2013). Taken together, these studies imply that the role of autophagy in tumorigenesis and progression is highly variable and correlated with timing, space and tumor microenvironment.

Induction of autophagy in cancer cells may serve an anti-cancer role by enhancing immunosurveillance. For example, in response to chemotherapeutic drugs, autophagy-competent tumors release the chromatin binding protein high mobility group B1 (HMGB1), calreticulin and adenosine triphosphate (ATP) that attract dendritic cells and T lymphocytes into the tumor microenvironment and promote anti-cancer responses (Michaud et al., 2011; Apetoh et al., 2007). In this study, we reveal that induction of autophagy by fluvastatin restricted the SPC-A-1 cells metastasis in nude mice; enhanced level of autophagy in cancer cells can attenuate the metastatic ability independent of adaptive immunity activation. Although we cannot exclude the possibility that autophagy-related innate immune responses are involved in clearance of SPC-A-1 cells, in-vitro experiments reveal that induction of autophagy by fluvastatin in these lung cancer cells greatly lowered their migratory and invasive ability without affecting the proliferation property. Therefore, induction of autophagy may serve an anti-cancer function in an immune-dependent or -independent way.

Metastasis is a risk for most cancer patients. Currently, there is no cure for bone metastasis, and the current treatment options using anti-bone metastatic agents have negative side effects. For example, bisphosphonates or denosumab treatments reduce tumor-associated SREs, but simultaneously increase the risk of the osteonecrosis in the jaw. In medicine, oncologists must make a difficult decision by weighing these benefits and risks to determine the best treatment regimen for the patients. Compared with bisphosphonates and denosumab, statins are frequently prescribed as cholesterol-lowering agents, and their safety has been well confirmed by more than a decade of medical practice. Furthermore, a clinical trial is needed to determine the efficacy of statins in the prevention of cancer bone metastasis. As a possible therapeutic treatment option, fluvastatin is promising to cancer patients with a high risk of bone metastasis.

Supplementary data to this article can be found online at http://dx.doi.org/10.1016/j.ebiom.2017.04.017.

Conflicts of Interest

The authors declare that they have no conflicts of interests.

Author Contributions

ZZY conceived the work and conducted some experiments. ZYS designed and conducted experiments, and drafted the manuscript. JPD designed some experiments and edited the manuscript. MYR and ZQY did the statistical analysis. Other authors conducted part of experiments in this manuscript.

Acknowledgements

This research was supported, in part, by grants from the National Natural Science Foundation of China (Nos. 81460440, 31670798, 81260322, 81372322 and 81560471), the National Key Research and Development Program of China, Stem Cell and Translational Research (2016YFA0100900), the Joint Special Funds for the Department of Science and Technology of Yunnan Province-Kunming Medical University (No. 2014FB059), the Scientific Research Projects from Internal Research Institutions of Medical and Health Units in Yunnan Province (Nos. 2014NS013, 2014NS014, 2014NS015 and 2014NS016), Foundation of the Yunnan Provincial Innovative Team of Bone and Soft Tissue Tumor (No. 2015HC026), Foundation of the Young and Middle-aged Academic and Technical Leaders of Yunnan Province (No. 2014HB034) and Doctor Scientific Research Startup Funds of the Third Affiliated Hospital of Kunming Medical University (No. BSJJ201406).

References

Apetoh, L., Ghiringhelli, F., Tesniere, A., Obeid, M., Ortiz, C., Criollo, A., et al., 2007. Toll-like receptor 4–dependent contribution of the immune system to anticancer chemotherapy and radiotherapy. Nat. Med. 13 (9), 1050–1059.

Araki, M., Maeda, M., Motojima, K., 2012. Hydrophobic statins induce autophagy and cell death in human rhabdomyosarcoma cells by depleting geranylgeranyl diphosphate. Eur. J. Pharmacol. 674 (2), 95–103.

Bamias, A., Kastritis, E., Bamia, C., Moulopoulos, L.A., Melakopoulos, I., Bozas, G., et al., 2005. Osteonecrosis of the jaw in cancer after treatment with bisphosphonates: incidence and risk factors. J. Clin. Oncol. 23 (34), 8580–8587.

Campbell, M.J., Esserman, L.J., Zhou, Y., Shoemaker, M., Lobo, M., Borman, E., et al., 2006. Breast cancer growth prevention by statins. Cancer Res. 66 (17), 8707–8714.
Castillo, K., Valenzuela, V., Matus, S., Nassif, M., Oñate, M., Fuentealba, Y., et al., 2013. Measurement of autophagy flux in the nervous system in vivo. Cell Death Dis. 4 (11), e917.
Chiang, G.G., Abraham, R.T., 2005. Phosphorylation of mammalian target of rapamycin (mTOR) at Ser-2448 is mediated by p70S6 kinase. J. Biol. Chem. 280 (27), 25485–25490.
Clendening, J., Penn, L., 2012. Targeting tumor cell metabolism with statins. Oncogene 31 (48), 4967–4978.
Collisson, E.A., Kleer, C., Wu, M., De, A., Gambhir, S.S., Merajver, S.D., et al., 2003. Atorvastatin prevents RhoC isoprenylation, invasion, and metastasis in human melanoma cells. Mol. Cancer Ther. 2 (10), 941–948.
Fizazi, K., Carducci, M., Smith, M., Damião, R., Brown, J., Karsh, L., et al., 2011. Denosumab versus zoledronic acid for treatment of bone metastases in men with castration-resistant prostate cancer: a randomised, double-blind study. Lancet 377 (9768), 813–822.
Freed-Pastor, W.A., Mizuno, H., Zhao, X., Langerød, A., Moon, S.-H., Rodriguez-Barrueco, R., et al., 2012. Mutant p53 disrupts mammary tissue architecture via the mevalonate pathway. Cell 148 (1), 244–258.
Hamilton, R.J., Morilla, D., Cabrera, F., Leapman, M., Chen, L.Y., Bernstein, M., et al., 2014. The association between statin medication and progression after surgery for localized renal cell carcinoma. J. Urol. 191 (4), 914–919.
Hindler, K., Cleeland, C.S., Rivera, E., Collard, C.D., 2006. The role of statins in cancer therapy. Oncologist 11 (3), 306–315.
Hu, Z., Gerseny, H., Zhang, Z., Chen, Y.-J., Berg, A., Zhang, Z., et al., 2011. Oncolytic adenovirus expressing soluble TGFβ receptor II-Fc-mediated inhibition of established bone metastases: a safe and effective systemic therapeutic approach for breast cancer. Mol. Ther. 19 (9), 1609–1618.
Jin, S., 2005. p53, autophagy and tumor suppression. Autophagy 1 (3), 171–173.
Kang, M., Jeong, C.W., Ku, J.H., Kwak, C., Kim, H.H., 2014. Inhibition of autophagy potentiates atorvastatin-induced apoptotic cell death in human bladder cancer cells in vitro. Int. J. Mol. Sci. 15 (5), 8106–8121.
Kenific, C.M., Thorburn, A., Debnath, J., 2010. Autophagy and metastasis: another double-edged sword. Curr. Opin. Cell Biol. 22 (2), 241–245.
Kuo, P.-L., Liao, S.-H., Hung, J.-Y., Huang, M.-S., Hsu, Y.-L., 2013. MicroRNA-33a functions as a bone metastasis suppressor in lung cancer by targeting parathyroid hormone related protein. Biochimica et Biophysica Acta 1830 (6), 3756–3766.
Kusama, T., Mukai, M., Iwasaki, T., Tatsuta, M., Matsumoto, Y., Akedo, H., et al., 2001. Inhibition of epidermal growth factor-induced RhoA translocation and invasion of human pancreatic cancer cells by 3-hydroxy-3-methylglutaryl-coenzyme a reductase inhibitors. Cancer Res. 61 (12), 4885.
Lopez-Olivo, M.A., Shah, N.A., Pratt, G., Risser, J.M., Symanski, E., Suarez-Almazor, M.E., 2012. Bisphosphonates in the treatment of patients with lung cancer and metastatic bone disease: a systematic review and meta-analysis. Support. Care Cancer 20 (11), 2985–2998.
Maiuri, M.C., Galluzzi, L., Morselli, E., Kepp, O., Malik, S.A., Kroemer, G., 2010. Autophagy regulation by p53. Curr. Opin. Cell Biol. 22 (2), 181–185.
McLeod, N.M., Brennan, P.A., Ruggiero, S.L., 2012. Bisphosphonate osteonecrosis of the jaw: a historical and contemporary review. Surgeon 10 (1), 36–42.
Michaud, M., Martins, I., Sukkurwala, A.Q., Adjemian, S., Ma, Y., Pellegatti, P., et al., 2011. Autophagy-dependent anticancer immune responses induced by chemotherapeutic agents in mice. Science 334 (6062), 1573–1577.
Misirkic, M., Janjetovic, K., Vucicevic, L., Tovilovic, G., Ristic, B., Vilimanovich, U., et al., 2012. Inhibition of AMPK-dependent autophagy enhances in vitro antiglioma effect of simvastatin. Pharmacol. Res. 65 (1), 111–119.
Muller, P.A., Vousden, K.H., 2013. p53 mutations in cancer. Nat. Cell Biol. 15 (1), 2–8.
Nielsen, S.F., Nordestgaard, B.G., Bojesen, S.E., 2012. Statin use and reduced cancer-related mortality. New Engl. J. Med. 367 (19), 1792–1802.
Parikh, A., Childress, C., Deitrick, K., Lin, Q., Rukstalis, D., Yang, W., 2010. Statin-induced autophagy by inhibition of geranylgeranyl biosynthesis in prostate cancer PC3 cells. Prostate 70 (9), 971–981.
Peng, Y.-F., Shi, Y.-H., Ding, Z.-B., Ke, A.-W., Gu, C.-Y., Hui, B., et al., 2013. Autophagy inhibition suppresses pulmonary metastasis of HCC in mice via impairing anoikis resistance and colonization of HCC cells. Autophagy 9 (12), 2056–2068.
Pich, C., Teiti, I., Rochaix, P., Mariamé, B., Couderc, B., Favre, G., et al., 2013. Statins reduce melanoma development and metastasis through MICA overexpression. Front. Immunol. 4.
Qiang, L., He, Y.-Y., 2014. Autophagy deficiency stabilizes TWIST1 to promote epithelial-mesenchymal transition. Autophagy 10 (10), 1864–1865.
Rocco, J.W., Leong, C.-O., Kuperwasser, N., DeYoung, M.P., Ellisen, L.W., 2006. p63 mediates survival in squamous cell carcinoma by suppression of p73-dependent apoptosis. Cancer Cell 9 (1), 45–56.
Rosenfeldt, M.T., O'Prey, J., Morton, J.P., Nixon, C., MacKay, G., Mrowinska, A., et al., 2013. p53 status determines the role of autophagy in pancreatic tumour development. Nature 504 (7479), 296–300.
Rove, K.O., Crawford, E.D., 2009. Metastatic cancer in solid tumors and clinical outcome: skeletal-related events. Oncology 23 (5), 21.
Scagliotti, G.V., Hirsh, V., Siena, S., Henry, D.H., Woll, P.J., Manegold, C., et al., 2012. Overall survival improvement in patients with lung cancer and bone metastases treated with denosumab versus zoledronic acid: subgroup analysis from a randomized phase 3 study. J. Thorac. Oncol. 7 (12), 1823–1829.
Sharifi, M.N., Mowers, E.E., Drake, L.E., Collier, C., Chen, H., Zamora, M., et al., 2016. Autophagy promotes focal adhesion disassembly and cell motility of metastatic tumor cells through the direct interaction of paxillin with LC3. Cell Rep. 15 (8), 1660–1672.
Siegel, R., Ward, E., Brawley, O., Jemal, A., 2011. The impact of eliminating socioeconomic and racial disparities on premature cancer deaths. CA 61 (4), 212–236.
Singh, S., Singh, P.P., Singh, A.G., Murad, M.H., Sanchez, W., 2013. Statins are associated with a reduced risk of hepatocellular cancer: a systematic review and meta-analysis. Gastroenterology 144 (2), 323–332.
Su, Z., Yang, Z., Xu, Y., Chen, Y., Yu, Q., 2015a. Apoptosis, autophagy, necroptosis, and cancer metastasis. Mol. Cancer 14 (1), 48.
Su, Z., Yang, Z., Xu, Y., Chen, Y., Yu, Q., 2015b. MicroRNAs in apoptosis, autophagy and necroptosis. Oncotarget 6 (11), 8474.
Suva, L.J., Washam, C., Nicholas, R.W., Griffin, R.J., 2011. Bone metastasis: mechanisms and therapeutic opportunities. Nat. Rev. Endocrinol. 7 (4), 208–218.
Tasdemir, E., Maiuri, M.C., Galluzzi, L., Vitale, I., Djavaheri-Mergny, M., D'Amelio, M., et al., 2008. Regulation of autophagy by cytoplasmic p53. Nat. Cell Biol. 10 (6), 676–687.
Taylor, K., Middlefell, L., Mizen, K., 2010. Osteonecrosis of the jaws induced by anti-RANK ligand therapy. Br. J. Oral Maxillofac. Surg. 48 (3), 221–223.
Tsubaki, M., Takeda, T., Kino, T., Obata, N., Itoh, T., Imano, M., et al., 2015. Statins improve survival by inhibiting spontaneous metastasis and tumor growth in a mouse melanoma model. Am. J. Cancer Res. 5 (10), 3186.
Wolfe, A.R., Debeb, B.G., Lacerda, L., Larson, R., Bambhroliya, A., Huang, X., et al., 2015. Simvastatin prevents triple-negative breast cancer metastasis in pre-clinical models through regulation of FOXO3a. Breast Cancer Res. Treat. 154 (3), 495–508.
Yang, P.M., Liu, Y.L., Lin, Y.C., Shun, C.T., Wu, M.S., Chen, C.C., 2010. Inhibition of autophagy enhances anticancer effects of atorvastatin in digestive malignancies. Cancer Res. 70 (19), 7699–7709.
Zhang, J., Yang, Z., Xie, L., Xu, L., Xu, D., Liu, X., 2013. Statins, autophagy and cancer metastasis. Int. J. Biochem. Cell Biol. 45 (3), 745–752.